Hindawi
Journal of Chemistry
Volume 2021, Article ID 5552187, 15 pages
https://doi.org/10.1155/2021/5552187

Research Article

Hybrid Cu-Fe/ZSM-5 Catalyst Prepared by Liquid Ion-Exchange for NO_x Removal by NH_3-SCR Process

Tuan Doan, Anh Dang, Dat Nguyen, Thanh Huyen Vuong, Minh Thang Le, and Huyen Pham Thanh

School of Chemical Engineering, Hanoi University of Science and Technology, 1 Dai Co Viet, Hanoi 100000, Vietnam

Correspondence should be addressed to Huyen Pham Thanh; huyen.phamthanh@hust.edu.vn

Received 22 January 2021; Revised 21 May 2021; Accepted 21 June 2021; Published 29 June 2021

Academic Editor: Jamal Rafique

A series of Cu/ZSM-5, Fe/ZSM-5, and Cu-Fe/ZSM-5 catalysts (Si/Al in ZSM-5 = 25) were prepared by different metal loadings using the liquid ion-exchange method. Several characterization methods were conducted to explore the effects of metals on the physical and chemical properties of catalysts. Meanwhile, the electron paramagnetic resonance method is also used to assess the copper and/or iron elements' coordination and valence state at intersections or in channels of ZSM-5. The metal-loading effects of all catalysts on the catalytic activities were studied for the removal of NO_x in a fixed-bed flow reactor using selective catalytic reduction with ammonia (NH_3-SCR). The results showed that the iron's addition could markedly broaden the operation temperature range of the Cu/ZSM-5 catalyst for NH_3-SCR between 200 and 550°C due to the presence of more isolated Cu^{2+} ions as well as additional oligomeric Fe^{3+} active sites and Fe_xO_y oligomeric species. This paper gives a facile and straightforward way to synthesize the practical-promising catalyst applied in NH_3-SCR technology to control NO_x emissions.

1. Introduction

Under industrialization with the industry's rapid growth, environmental problems are also accumulating and increasing swiftly, making the community concerned. Specifically, pollutants in the atmosphere have become significant perils to human health. Therefore, air pollution control is one of the urgent issues for industrial countries and all over the world. The scientific demonstration of the polluting properties of several chemical compounds has paved the way for more rigorous regulations to control their emissions. There are lots of causes for this problem, but the contribution of motorized traffic plays an important role. Based on each chemical compound's polluting properties, different laws are in place to control their emissions. In particular, the exhaust from the internal combustion engine contributes mainly to this problem. The vital pollutant compounds are incombustible hydrocarbon (HC), carbon monoxide (CO), particulate matter (PM), and nitrogen oxide (NO_x) emissions, which are primarily due to spontaneous oxidation of NO [1]. Accordingly, one of the most notable air pollutants is NO_x, which is obtained mainly from emissions in stationary and mobile sources of high-temperature combustion and from electrical discharge during thunderstorms [2]. The prominent harmful effects of NO_x are acid rain formation, photochemical smog, ozone reduction, and fog.

Recently, with continuous efforts to satisfy more rigorous regulations on NO_x emissions in both mobile and stationary sources, several innovative technologies have been exploited in parallel with the application of disposable methods as the three-way catalyst, NO_x storage and reduction (NSR), and selective catalytic reduction (SCR) [3]. In particular, one of the most effective NO_x reduction technologies is NH_3-SCR, which is using NH_3 or aqueous urea as a reducing agent to convert NO_x to nitrogen [4]. This technology uses catalysts to assist in stimulating the reaction between NH_3 and NO_x to produce more quickly harmless N_2 and H_2O productions as the following reaction [5]:

$$4NH_3 + 4NO + O_2 \longrightarrow 4N_2 + 6H_2O \quad (1)$$

Until now, NH_3-SCR technology has been applied with a wide variety of catalysts such as precious metals, metal

oxides, and zeolite-based catalysts [1]. The catalysts used in this technology are of the utmost importance with lots of particular requirements. For instance, to accommodate exhaust emissions from both light and heavy diesel engines and to increase the N_2 selectivity of the NO_x reduction reaction, the catalyst must have a wide operating temperature range (i.e., from 100 to 600°C). Besides, it also needs to be stabilized in water vapor and sulfur oxides generated from fuel combustion [3]. Consequently, the improvement of catalyst properties to enhance their efficiency in the SCR method has been increasingly studied. In particular, the most promising alternative to the currently common-use commercial catalyst as vanadium-based catalysts is the combination of zeolite-based catalysts and different transition metals such as Fe, Cu, Mo, and Cr [3]. The well-recognized CHA-structural zeolites for a deNOx application might be called SSZ-13 in particular, but the synthesis with a costly prototype is the key constraint on process commercialization of the SSZ-13 (N, N, N-trimethyl-l-adamantammonium hydroxide) [6, 7]. This disadvantage, on the other hand, could be overcome by using ZSM-5, whose synthesis is more economical and convenient. Specifically, the highly active iron and copper-denatured ZSM-5 catalyst has received more and more attention recently [8–10]. ZSM-5 is a nanometer-sized pore-structured molecular sieve material with strong acid sites that can adsorb NH_3 onto the surface and converts them to NH_4^+. Also, the individual characteristic activity of this catalyst in the SCR reaction is shown through a miniature "nanoreactor" that exists in the internal space, providing a favorable reaction space and an electronic environment to create highly dispersed transition metal oxide clusters [11]. The advantage of forming oxide clusters and nanoparticles can be explained by the ultrasonic cavitation effect. It can support the dispersion of the active component inside micropores of ZSM-5 and diminish the relative supersaturation of solution leading to the inhibition of secondary nucleation of precursors and extra development of the crystal nucleus. Thus, the catalyst based on ZSM-5 shows outstanding catalytic activity at the low-temperature range due to the creation of more active centers through the impact of oxide clusters and nanoparticles.

It has been reported that Cu-exchanged to zeolites exhibited more activity below 300°C; when the temperature is above 350°C, the NO conversion is decreased due to the oxidation of ammonia. Meanwhile, Fe-doped zeolite gave better activity for NH_3-SCR at high temperatures [4]. However, there is still an open discussion concerning the nuclearity and identity of Fe and Cu active sites for NH_3-SCR reaction. Chronologically, the Cu-based zeolite is the first metal loading on zeolite discovered active in the SCR reaction. It is generally admitted that both the copper oxo cations and Cu^{2+} ions, which are active sites in this catalyst, play an important role in the deNOx process [1, 12]. In opposition to the Cu-zeolite system, the Fe-zeolite system submitted multiple active sites such as intrazeolite binuclear Fe-oxo, isolated Fe^{2+} and Fe^{3+} ions, small Fe_xO_y clusters, or oxygen bridged binuclear iron species $[HO–Fe–O–Fe–OH]^{2+}$, groups of a wide range of nuclearity and large sets of oxides [13–15]. Nowadays, bimetal catalysts based on zeolites have attracted much attention, especially codoping of Cu and Fe supported on zeolite, which became a promising catalyst for the NH_3-SCR reaction. Recent research has indicated that such materials show higher NO_x removal efficiency over a more extended temperature range than with individual Fe- or Cu-based zeolite catalysts [16–18]. Iron and copper's simultaneous appearance promotes more acid sites, an alteration of electronic properties, and augmentation of redox ability than for a single metal catalyst.

This study aims to clarify the application of copper-iron bimetallic-supported commercial ZSM-5 for the NH_3-SCR catalyst. Additionally, Cu-Fe/ZSM-5 samples were compared with single metal on ZSM-5 (Cu/ZSM-5 and Fe/ZSM-5), thereby clarifying supplementary advantages, reciprocal effects of both copper and iron to catalytic properties, and the ability to widen the operating temperature range for deNOx with NH_3 reductant. In this work, the aqueous ion-exchange method was applied for preparing all the metal catalysts. The Cu-Fe/ZSM-5, Cu/ZSM-5, and Fe/ZSM-5 catalysts were characterized by various techniques to determine the physicochemical properties. The main objective of this study focuses on the following contents:

(i) The effects of Cu, Fe, and codoping Cu-Fe supported on ZSM-5 zeolite to their catalyst properties were clarified

(ii) Also, the NH_3-SCR activity and the hydrothermal durability of catalysts were conducted

2. Experimental

2.1. Catalyst Preparation. Metals (Cu and/or Fe) were added to ZSM-5 (DNH-Z, $SiO_2/Al_2O_3 = 25$ of Tosoh Corporation) through a two-step liquid ion-exchange process. In the first step, ZSM-5 was changed into ammonium form by exchanging with ammonium acetate (CH_3COONH_4, Sigma-Aldrich) solution two times. The first exchange period was the continuous agitation of ZSM-5 zeolite with solid ammonium acetate and purified water at 80°C for 5 hours; then the substantial part was gathered by centrifugation. After that, the same process was performed one more time, but with a discrepancy in exchange time (18 hours) and stirring at room temperature. The centrifuged solid portion was subsequently dried at 120°C to accomplish NH_4^+/ZSM-5 powders. In the second step, the ammonium form of ZSM-5 was ion-exchanged with metals, in which Cu and/or Fe were doped using $Cu(CH_3COO)_2.H_2O$ (Sigma-Aldrich) and/or $Fe(CH_3COO)_2.4H_2O$ (Sigma-Aldrich), respectively. The solution was mixed continuously at room temperature within 24 hours and then centrifuged and washed with distilled water to reach a solid component. The collected part was then dried at 120°C for the night and calcined at 550°C for 5 hours in the flow of 20% O_2/Ar. The ZSM-5 catalyst samples were denoted as xCu/ZSM-5, yFe/ZSM-5, and xCu-yFe/ZSM-5 in which x and y are the weight percentage of Cu and/or Fe used in synthesis, respectively.

2.2. Characterizations. All characterization methods have been effectuated for as-calcined samples. Powder X-ray

diffractometer Bruker D8 with Cu-Kα radiation ($\lambda = 1.5418$ Å) at a scanning speed of 1°/min within $2\theta = 5$–$50°$ was used to achieve the X-ray diffraction (XRD) patterns of catalysts. The field emission scanning electron microscopy (FE-SEM) was performed on Hitachi S-4800 (Japan) to explore the samples' different morphology. Simultaneously, the chemical compositions of the catalysts were also determined by the Hitachi S-4800 (Japan) machine equipped with an energy-dispersive X-ray spectrometer (EDS). Measurements of nitrogen adsorption-desorption were performed at −196°C using a Micromeritics Analyzers ASAP 2020. The samples were degassed under a vacuum at 300°C before the examination. The overall surface area was evaluated based on the Brunauer–Emmette–Teller (BET) theory and t-plot for external surface and surface and volume. UV-Vis diffuse reflectance spectra (UV-Vis DRS) were performed on an Avantes Avaspec-ULS2048XL-EVO spectrometer equipped with an integrating sphere coated with $BaSO_4$, from 200 to 1000 nm, and the program AvaSoft 8 was used. The different copper and iron species were quantified by the area ratios of the respective subbands relative to each other [19]. Temperature-programmed desorption of ammonia (NH_3-TPD) experiments for the surface acidity determination were performed on a Micromeritics Auto Chem 2920 instrument. The TPD measurements were conducted in He flow (30 mL/min), and the temperature was increased from 100 to 600°C with a heating rate of 10°C/min. Besides, the temperature-programmed reduction with H_2 (H_2-TPR) was also carried out on Micromeritics Auto Chem 2920 instrument. In the initial, 0.1 g of the catalyst was placed into the quartz U-shaped microreactor and pretreated in He at 300°C for 1 hour, followed by cooling down to 50°C before the acquisition. Afterward, the ramping program was processed by the flow of 10 vol% H_2/He from 50 to 900°C (30 mL/min), with a heating rate of 10°C/min. A detector continuously collected the signals during this process. Additionally, the reactor's cooling trap was positioned next to the experiment to prevent the byproducts of experiments (i.e., H_2O, CO_2) from seeping into the detector. Electron paramagnetic resonance (EPR) spectra were performed on the Bruker EMX-Micro-EPR spectrometer, with a continuous wave X-band, using a microwave power of 6.3 mW, a modulation frequency of 100 kHz, an amplitude of 0.5 mT, and a magnetic field of 1000–5000 G.

2.3. Catalytic Performance. The catalytic activity test of all catalysts for the NH_3-SCR reaction was carried out in a fixed-bed quartz reactor working under a steady flow mode with ABB Gas Analyzer AO2020 Limas21 (UV sensor) spectrometer in the condition of excess oxygen (Figure 1). For each activity test, 100 mg catalyst (40–60 mesh) and the total flow rate of 200 mL/min were used, leading to the gaseous hourly space velocity of 120 000 h^{-1}. Moreover, to minimize condensation in downstream tubing, all the gas lines were heated and kept at approximately 100°C. In this reaction system, the used reactant gas has a composition of 1000 ppm NO, 1000 ppm NH_3, 8 vol% O_2, and Ar as balance. The temperature range of the reaction was from 200°C to 550°C. Firstly, the catalyst was activated in a flow of 20% O_2/Ar at 550°C for 1 hour. At each temperature, the expected time to obtain a steady state was about 1 hour. A similar condition was followed for the NH_3 oxidation reaction, where NO was not added to the gas mixture. In the investigation of hydrothermal stability, the catalysts were aged in a quartz tube reactor at 650°C or 750°C in 10% H_2O/air under a total flow rate of 1 L/min for 24 hours before the activity test. When the system was already stable, calculation of the NO and NH_3 conversions was performed through the inlet and outlet gas contents by the following equations:

$$NO_x \text{ conversion}\,(\%) = \frac{C_{NO_x\text{inlet}} - C_{NO_x\text{outlet}}}{C_{NO_x\text{outlet}}} \times 100\% \quad (2)$$

$$NH_3 \text{ conversion}\,(\%) = \frac{C_{NH_3\text{inlet}} - C_{NH_3\text{outlet}}}{C_{NH_3\text{outlet}}} \times 100\% \quad (3)$$

3. Results and Discussion

3.1. Structure and Texture of Catalysts. The catalysts' structure investigated by the XRD method is presented in Figure 2. In JCPDS data cards (JCPDS 42-0024), which show peak diffractions at 7.92°, 8.80°, 14.78°, 23.10°, 23.90°, and 24.40°, the prevalent diffraction peaks for commercial ZSM-5 can be simple to index into the standard parameters for MFI topology. The XRD patterns of all catalysts have included all characteristic peaks corresponding to ZSM-5, suggesting that ZSM-5 does not destroy its original form during the process of aqueous ion-exchange and calcination [20]. However, in contrast to those of the parent sample, the intensities of Fe/ZSM-5, Cu/ZSM-5, and Cu-Fe/ZSM-5 decrease due to the higher absorption coefficient of metal compounds for X-ray radiation or treatment with neutral aqueous solutions [21].

We can claim safely from Table 1, in conjunction with the chemical composition, that the synthesized materials are Fe- and Cu-containing ZSM-5-zeolites. No diffraction peaks were found at either metal and/or to metal oxide clusters, indicating that the copper and/or iron formed species are well distributed and within the range of nanometers [22]. Interestingly, the Cu-Fe/ZSM-5 synthesized does not have a peak of diffraction like α-Fe_2O_3 and CuO_x. In contrast, its peak amplitude and corresponding crystallinity are slightly more significant than those of Cu/ZSM-5, as shown in Figure 2. This result indicates that incorporating Cu and Fe in ZSM-5 simultaneously could decrease the effects of a single metal onto ZSM-5. Furthermore, in all samples, the Na concentrations are below 0.09 wt.% (Table 1), which does not impact catalyst NH_3-SCR performance of the catalysts [23].

FE-SEM observed the morphological properties of the synthesized zeolites and the relevant photographs in Figure 3. It is apparent that the ZSM-5 parent primarily consists of bright polycrystalline aggregates, irregularly localized, and distinct edged in the typical geometry [24]. Moreover, after doping metal(s), the primary morphology for all catalysts

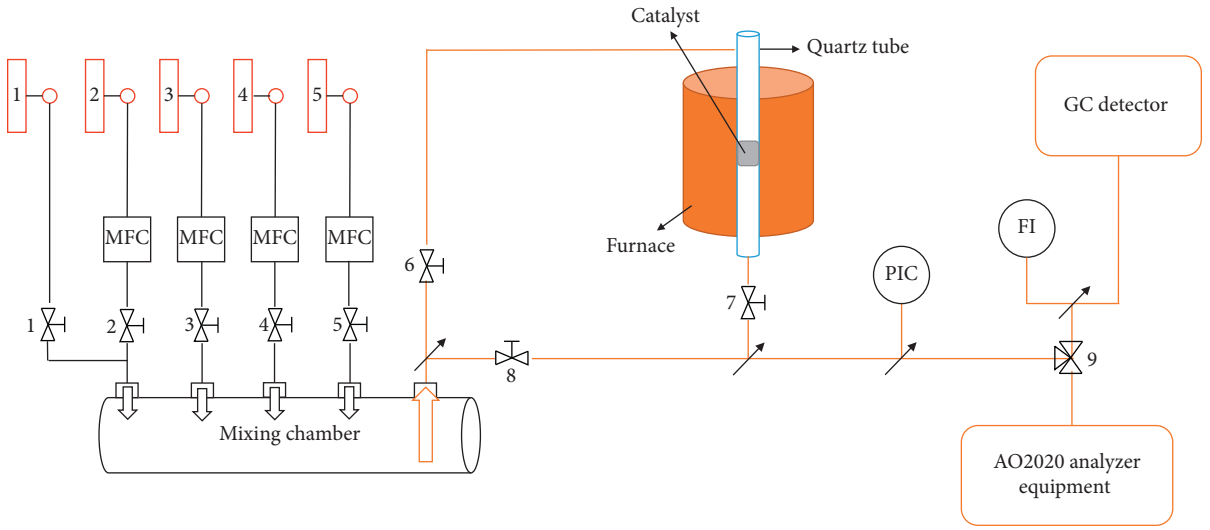

Figure 1: Schematic diagram of the experimental apparatus for activity test.

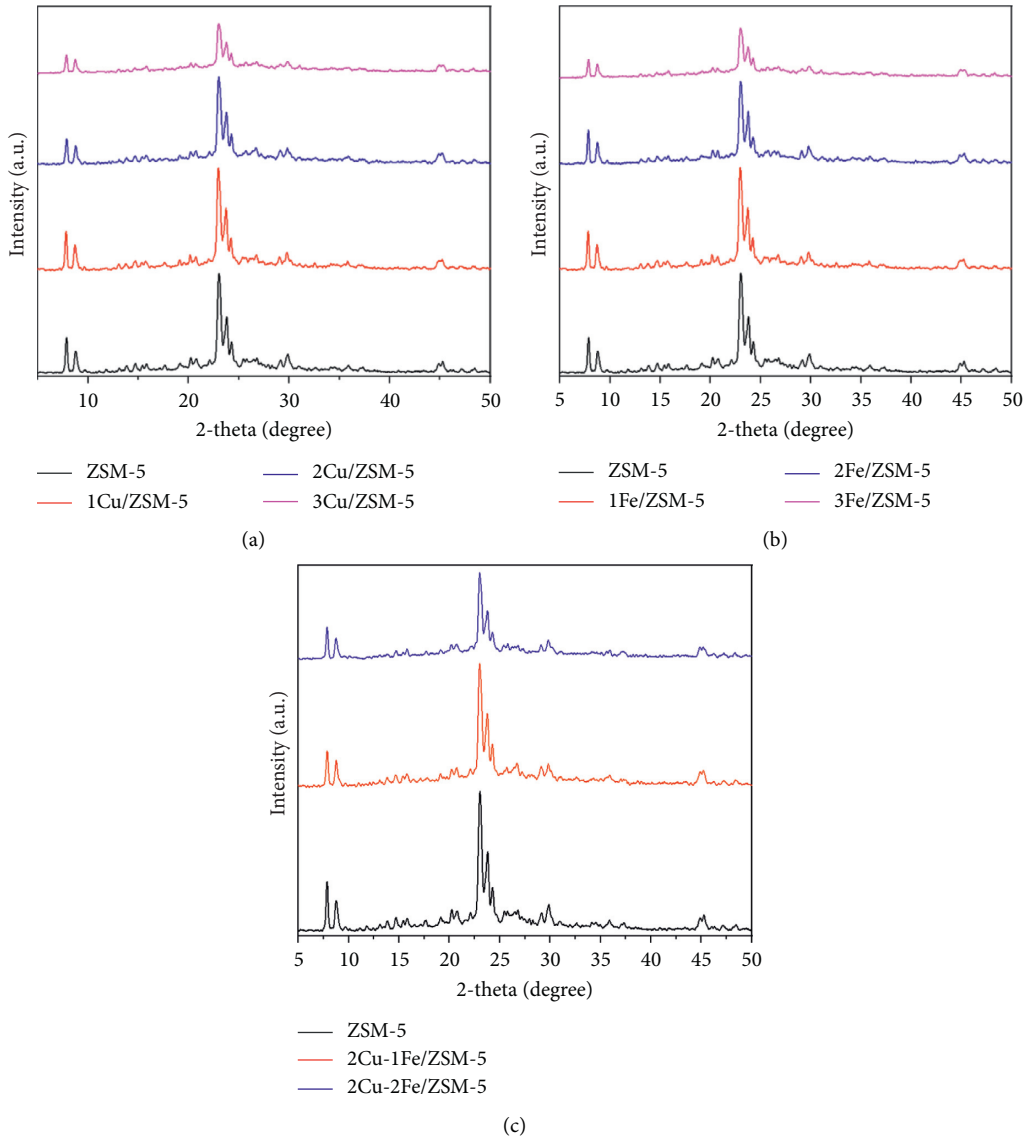

Figure 2: XRD patterns of (a) Cu/ZSM-5, (b) Fe/ZSM-5, and (c) Cu-Fe/ZSM-5.

Table 1: Fe, Cu, and Na amounts in all catalysts obtained by EDS.

Catalyst	Metal atomic concentration (wt.%)		
	Cu	Fe	Na
ZSM-5	—	—	0.075
1Cu/ZSM-5	0.97	—	0.079
2Cu/ZSM-5	1.92	—	0.077
3Cu/ZSM-5	2.89	—	0.075
1Fe/ZSM-5	—	0.92	0.073
2Fe/ZSM-5	—	1.91	0.080
3Fe/ZSM-5	—	2.78	0.074
2Cu-1Fe/ZSM-5	1.98	0.92	0.079
2Cu-2Fe/ZSM-5	1.91	1.93	0.078

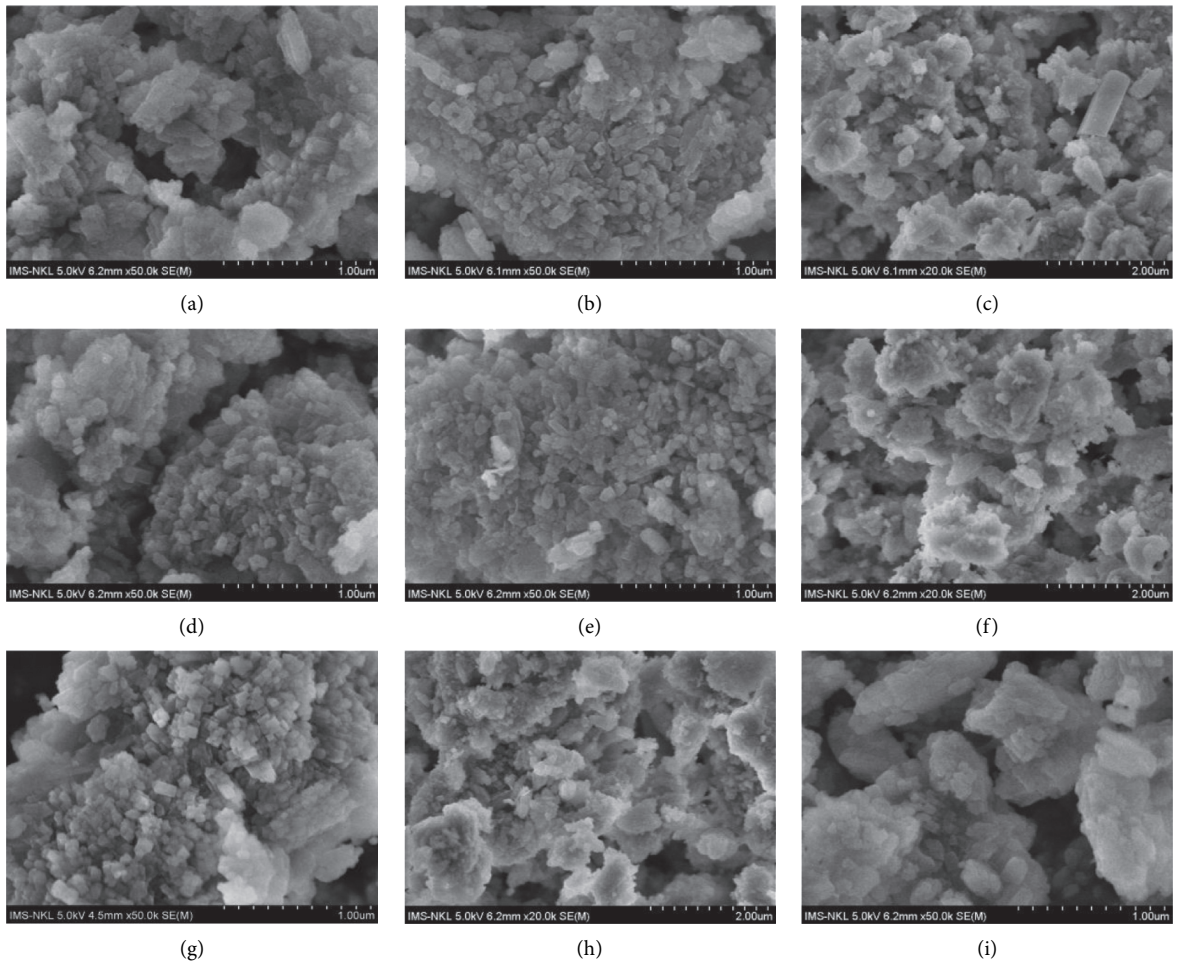

Figure 3: FE-SEM images of all catalysts. (a) 1Cu/ZSM-5. (b) 2Cu/ZSM-5. (c) 3Cu/ZSM-5. (d) 1Fe/ZSM-5. (e) 2Fe/ZSM-5. (f) 3Fe/ZSM-5. (g) 2Cu-1Fe/ZSM-5. (h) 2Cu-2Fe/ZSM-5. (i) ZSM-5.

remains almost unchanged. However, depending on the metal loading, small amounts of aggregates composed of nanosized particles, particularly in the high amount of metal loading that can be created during calcination, emerge from the primary morphology of Fe/ZSM-5, Cu/ZSM-5, and Cu-Fe/ZSM-5. Or Doan et al. note that the combined Cu_xO or α–Fe_2O_3 nanoparticles can be ascribed to particular layers of suspended matter [21]. Alongside the EDS results (Table 1) and the XRD patterns (Figure 2), this can be due to the fact that some large metal comprising agglomerations are well-distributed crystal metal oxide particles onto ZSM-5 composition. For Cu-Fe bimetal catalysts based on ZSM-5, which have a metal content of about three percent, the catalysts are smoother than the other two individual metal-fueled zeolites with a metal load of over two percent.

Nitrogen adsorption-desorption isotherms for all catalysts are shown in Figure 4. The ZSM-5, Fe/ZSM-5, Cu/ZSM-5, and Cu-Fe/ZSM-5 isotherms are categorized as category I,

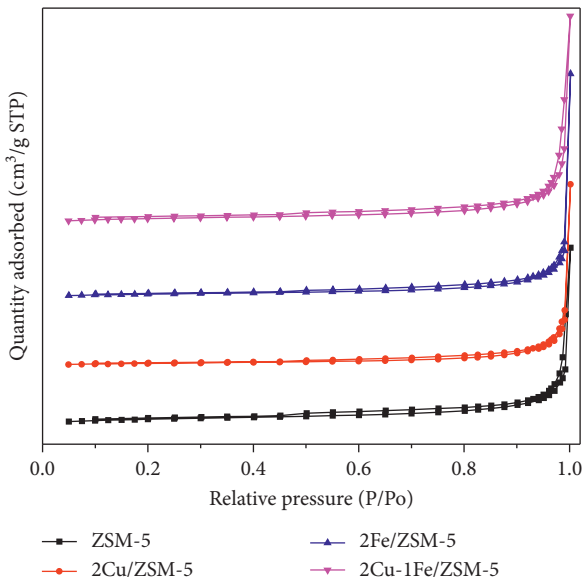

FIGURE 4: N_2 adsorption and desorption isotherms of catalysts.

characteristic of the micropores materials according to IUPAC classification. The nitrogen intake at about $P/P_0 = 0.01$ of all catalysts is close to that of the parent ZSM-5, indicating that the microporous is not greatly blocked during the preparation. Table 2 displays the significant textural properties of all nanocatalysts. The calculation of N_2 physisorption is a function of zeolites' topology, including S_{BET}, V_{pore}, and average pore diameter. It suggests that the ZSM-5 carrier has large surface areas and the active components could scatter well on the carrier through the liquid ion-exchange technique. As seen in Table 2, metal species introduction had little effect on the textural properties of ZSM-5. Overall, a slight decrease in the BET surface area typically depends on the content and form of metal. However, V_{pore} is a little higher for all nanocatalysts than the ZSM-5. This is why urea alkaline environment-induced ZSM-5 particles split into smaller particles and thus increased pore volume [25]. Furthermore, a minor increase in pore diameter of ZSM-5 also resulted from metal loading. The explanation may be due to the dissociation of some boundaries in ZSM-5 because of the urea alkaline environment, and consequently, the pore diameter of all catalysts increased [25].

3.2. Chemisorption Results. The catalyst's surface acidity always makes a significant contribution to the NH_3-SCR reaction for the removal of NO_x [26]. This research also used the NH_3-TPD method to measure the strength and the number of acid sites in the prepared catalysts. The corresponding profiles are shown in Figure 5 and Table 3. Typically, NH_3 adsorption on weak, medium, and strong acid sites answers to the three distinct peaks at low (120–220°C), medium-high (250–380°C), and high (380–500°C) temperatures, respectively. Ammonia desorption at a lower temperature is related to weakly physisorbed NH_3 at Lewis acid sites. Oppositely, the high-temperature desorption peak is attributed to the adsorbed strongly NH_3 molecules on Brønsted acid sites [27, 28]. Although there are still many controversies, the assignment of the medium-high desorption peak is somehow attributed to NH_3 weakly adsorbed on Brønsted acid sites or associated with extra-framework Al [28]. These Brønsted and Lewis sites can be attributed to acidic protons and to extraframework Al atoms, which compensate framework Al atoms charge, respectively [29]. Consequently, it appears that the presence of Al atoms in ZSM-5 zeolite is in charge of the formation of centers for ammonia chemisorption. According to Table 3 and Figure 5, the doping of Cu and/or Fe into ZSM-5 decreases the acidity of ZSM-5. In comparison with ZSM-5, sites for NH_3 chemisorption are less generated over metal introduction into the catalyst due to the replacement of Brønsted acid protons by metal [30]. Compared to individual Fe-doped ZSM-5, both strength and acid amounts of the strong acid sites are slightly decreased when codoping Cu and Fe together. In this case, it is assigned to the incorporation of Fe into the framework of Cu-Fe/ZSM-5 [31]. It was reported that the strength and acid amount of the strong acid sites is an essential factor for the adsorption of NH_3. Therefore, it influences the NH_3-SCR activity significantly [32]. With a suitable number of acid sites on Cu-Fe/ZSM-5, the catalytic activity may be further enhanced, and thus, it is more beneficial for the SCR reaction [33].

The H_2-TPR profiles of Fe/ZSM-5, Cu/ZSM-5, and Cu-Fe/ZSM-5 catalysts are shown in Figure 6 to understand the redox proprieties of the catalysts better. There can be three H_2 consumption zones observed in the TPR pattern of the Cu/ZSM-5 catalyst: the first peak at 180°C is corresponding to the reduction of external surface nanosized CuO to Cu^+ [34], the second sharp peak at about 250°C is related to the reduction of isolated Cu^{2+} ions to Cu^+ in ion-exchange positions of zeolites, and another one located at 370°C as a trace, can be assigned to the reduction of CuO particles to Cu^0 and Cu^+ to Cu^0 [35]. According to the high copper content, the excess amount of copper is detected as CuO when the exchange sites have been involved. One primary peak of the Fe/ZSM-5 catalyst at around 470°C ascribes to the reduction of Fe^{3+} to Fe^{2+} at zeolite ion-exchange positions [36, 37] as well as the reduction of Fe_2O_3 to Fe_3O_4 [38]. Also, a small and broad peak attended at approximately 630°C, which can refer to the reduction of Fe_3O_4 to FeO [39] and a residual fraction of framework Fe^{3+} that is hardly reduced [40]. Krishna et al. [41] reported that if there have been extended FeO_x phases, they commonly point to reduction peaks around 600°C. Ariel Guzmán-Vargas et al. [39] based on different temperature-programmed reduction studies of Fe/ZSM-5 arranged that the peak for hydrogen consumption met at around 430°C can be associated with the reduction of Fe^{3+} to Fe^{2+} in Fe species by the framework-charge compensation. When Cu and Fe are doped simultaneously into ZSM-5, the results showed a transition of the first reduction peak to a higher temperature than Cu/ZSM-5. This change is due to the strong interaction between copper and iron metallic components and the integration in Cu-Fe/ZSM-5, making them harder to reduce. Moreover, the peak centered at 420°C relates to the reduction of Fe species [17],

Table 2: The main textural properties of all catalysts.

Catalyst	BET surface area (m^2/g)	Average pore diameter (nm)	Pore volume (cm^3/g)
ZSM-5	397	0.45	0.25
1Cu/ZSM-5	383	0.47	0.32
2Cu/ZSM-5	301	0.48	0.34
3Cu/ZSM-5	257	0.50	0.35
1Fe/ZSM-5	355	0.52	0.28
2Fe/ZSM-5	287	0.54	0.29
3Fe/ZSM-5	232	0.55	0.31
2Cu-1Fe/ZSM-5	339	0.49	0.35
2Cu-2Fe/ZSM-5	259	0.51	0.32

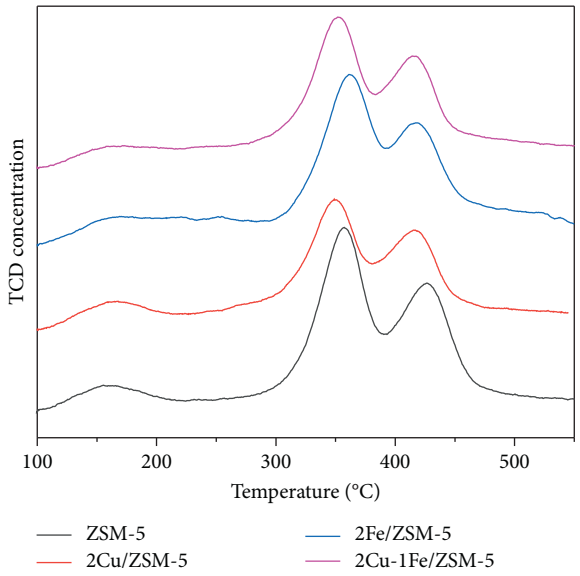

Figure 5: Temperature-programmed desorption of ammonia of catalysts.

Table 3: Acidic properties of the catalysts.

Samples	Peak (mmol/g)			Total (mmol/g)
	Peak 1	Peak 2	Peak 3	
ZSM-5	0.65	1.18	1.05	2.88
2Cu/ZSM-5	0.69	0.83	0.76	2.28
2Fe/ZSM-5	0.68	1.10	1.01	2.79
2Cu-1Fe/ZSM-5	0.57	0.95	0.89	2.41

leading to the appearance of the iron reduction peaks at high temperatures which become more self-evident, and the copper peaks become weaker. The broader peaks present after Fe loading demonstrates that Fe species had various forms. Thus, improving the redox proficiency of such Fe species can enhance the NO_x reduction effectiveness at high temperatures.

3.3. Cu and Fe Species onto ZSM-5. The UV-Vis DRS was also used to analyze the nature and coordination of copper and iron species in the catalysts and the respective spectra are compared in Figure 7. The spectra of Fe/ZSM-5, Cu/ZSM-5, and Cu-Fe/ZSM-5 are strikingly different, showing that the Fe and Cu species exist in distinct forms. The absorption peaks of around 270 nm are due to ZSM-5 zeolite [16]. In the Cu/ZSM-5 sample's spectra, the strong band at about 230 nm is assigned to the d – d transition of the charge-transfer band, which relates to the transition O ⟶ Cu from lattice oxygen to isolated Cu^{2+} ions [6]. In addition, the broad but less intense band between 650 and 850 nm in Cu/ZSM-5 and Cu-Fe/ZSM-5 relates to the d – d transition of Cu^{2+} ions in an octahedral environment due to the distributed CuO particles [42]. With the Fe species, the band below 300 nm confirms the existence of isolated iron ions in the structure of tetrahedrons or octahedrons. Besides, the signal between 300 and 400 nm refers to the Fe-oxo oligomers, and the peak higher than 400 nm is due to iron oxide aggregates [43]. In this research, the Fe/ZSM-5 pattern shows a band at 214 nm which is ascribed to the Fe intrusion instead of Fe^{3+} ions coordinated with the tetrahedra within the framework of the zeolites [44], and a band located at 390 nm relative to the oligo nuclear Fe_xO_y cluster [45, 46]. In the meantime, both Fe/ZSM-5 and Cu-Fe/ZSM-5 display an aggressive absorption band at 250 nm due to the charge transfer of oxygen to iron, explaining the presence of isolated Fe species entered into the zeolite framework in the tetrahedral coordination [47]. Moreover, the d-d transition of the quite-inactive factor of the NH_3-SCR as α-Fe_2O_3 also gives a band centered at 500 nm [48].

In order to analyze the state of iron and copper ions in our catalysts, EPR was conducted due to its powerful technique [49]. The obtained EPR spectra at −173°C are shown in Figure 8. In the EPR spectrum of copper samples, isolated Cu^{2+} presents a parallel signal with four adsorption peaks and a sharp peak in the vertical region [50]. On the other hand, Cu^{2+} species in dimeric species and Cu^{+} ions do not interact with this technique [50, 51]. This phenomenon is due to the fact that isolated Cu^{2+} ions owned a nuclear spin (I = 3/2) and the 3d unpaired electrons coupled with each other. The EPR spectra of the samples were simulated using the software package EasySpin implemented in MATLAB [52]. In the results shown in Figure 8(a), all Cu/ZSM-5 samples exhibit an axial EPR spectrum of isolated Cu^{2+} ions with resolved hyperfine structure with $g_{||} = 2.389$, $A_{||} = 400$ MHz, $g\perp = 2.095$, and $A\perp = 57$ MHz. This has been assigned to copper species close to the channel intersection in several zeolites, for example, hydrated Cu-BEA and Cu-MFI [53]. Increasing the amount of doped Cu from 1 wt.% to 2 wt.% leads to a significant increase in the axial signal's intensity, indicating the formation of more isolated Cu^{2+}

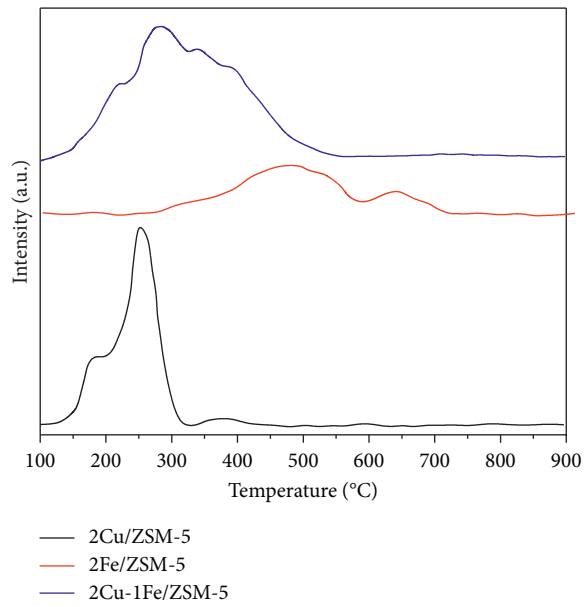

Figure 6: H_2-TPR profiles of catalyst samples.

ions (25.5% in the sample 2Cu/ZSM-5 compared to 21.5% in the sample 1Cu/ZSM-5). However, with higher Cu content of 3 wt.%, the amount of isolated Cu^{2+} species decreases to 17.5%. Besides, the isotropic signal at $g = 2.17$ in the sample 3Cu/ZSM-5 is also broader. This broad signal is related to the magnetically interacting Cu^{2+} species in dimeric species and such Cu sites located in close vicinity or CuO clusters.

Figure 8(b) illustrates the EPR spectra of Fe/ZSM-5 samples recorded at −173°C. It is clear to see that iron species give three different EPR signals, containing a low-field shoulder at $g = 4.23$ and two broader signals at $g = 2.29$ and $g = 2.05$. To be more specific, the signal at $g = 4.23$ is attributed to strong rhombic, highly distorted isolated Fe^{3+} species and higher coordination numbers. This could be due to the isolated iron monomers located paramagnetically at ion-exchange positions inside the zeolite micropores [54]. The weak low-field line $g = 2.29$ and 2.05 signal might be an axial stack of distorted Fe^{3+} monomers and/or for interacting octahedrally with residual Fe_2O_3 phase [54]. Another observation made from the spectrum is that the intensity of EPR signals was raised significantly when increasing the content of Fe doping, especially with samples containing more than 1 wt.% of Fe loading. In other words, the higher intensity of the signals at $g = 2.29$ and $g = 2.05$ in these samples suggests the presence of more clustered Fe oxides.

As shown in Figure 8(c), compared to the monometal catalysts, EPR signals of bimetallic catalysts exhibit dominant axial signals from isolated Cu^{2+} sites. Compared to the same amount of copper loading in monocopper catalysts, the intensity of isolated Cu^{2+} in 2Cu-1Fe/ZSM-5 was increased while that of 2Cu-2Fe/ZSM-5 was lower. This behavior suggests that a suitable content of iron could lead to the formation of a higher amount of isolated Cu^{2+} ions. Moreover, increasing the amount of Fe loading in bimetallic catalysts could reveal the signals of isolated Fe^{3+} in tetrahedral coordination at $g = 4.23$. Meanwhile, the appearance of Fe_xO_y clusters cannot be shown given that their signals at $g = 2.29$ and 2.05 might be covered by the isolated active Cu^{2+} signal.

3.4. Catalyst Performance. The catalytic performance of the prepared catalysts has been evaluated in SCR of NO with NH_3 and is shown in Figure 9 in a microcatalytic flow reactor. The conversion of NOx with Cu/ZSM-5 samples in Figure 9(a) dramatically improves from 250°C to 300°C and stays above 80% between 300°C and 450°C, particularly in the 300–400°C range when the yield achieves over 90%. Later, the conversion of NO_x decreases steadily above 400°C and only exceeds 58% at 550°C. Among copper-loaded samples, the sample with 2 wt.% Cu shows the highest activity. Fe/ZSM-5 samples' catalytic efficiency reveals, as seen in Figure 9(b), that the addition of iron in ZSM-5 increases the SCR reaction slightly over the whole temperature range. However, a decent range of temperatures from 400 to 500°C could only be obtained, which is typical of the Fe-zeolite mechanism with maximal operation at high temperatures [2]. Higher Fe content (up to 3 wt.%) NO_x conversion tends to a slight decrease at high temperatures. These findings suggest that higher metal loading could have a detrimental impact on conversions of NO_x. Therefore, selection for the content of the doped metal is necessary to enhance the removal of NO_x. In summary, the results of Figures 9(a) and 9(b) show that sufficient metal content might support the conversion of NO_x while excessive Cu or Fe loads may block the zeolite channel. This could be investigated in Figure 4 and Table 2 by the result of N_2 adsorption-desorption.

When incorporating both Cu and Fe into ZSM-5, 2Cu-1Fe/ZSM-5 catalyst significantly enhances the NO_x conversion in the broader temperature range of 350–550°C, while 2Cu-2Fe/ZSM-5 sample only presents a temperature

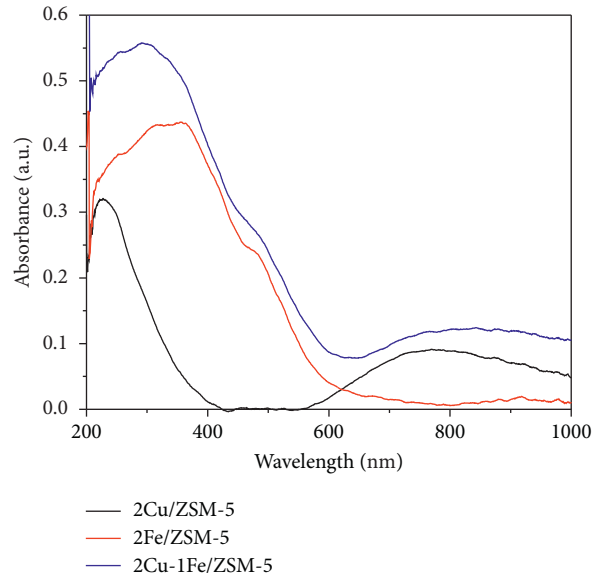

Figure 7: UV-Vis DRS spectra of the catalysts.

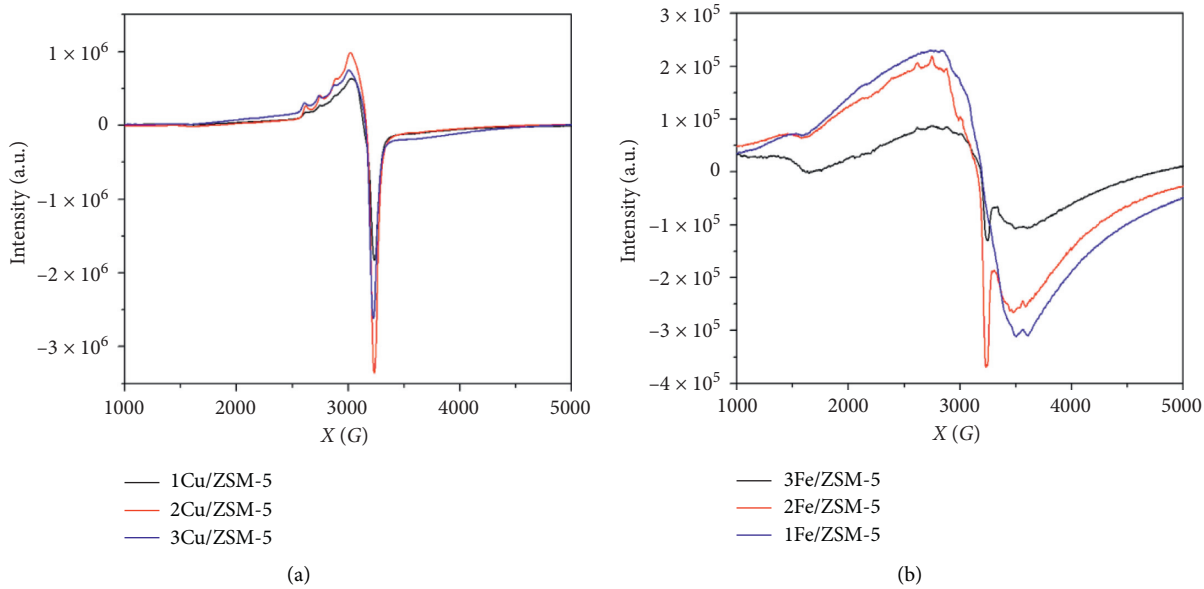

Figure 8: Continued.

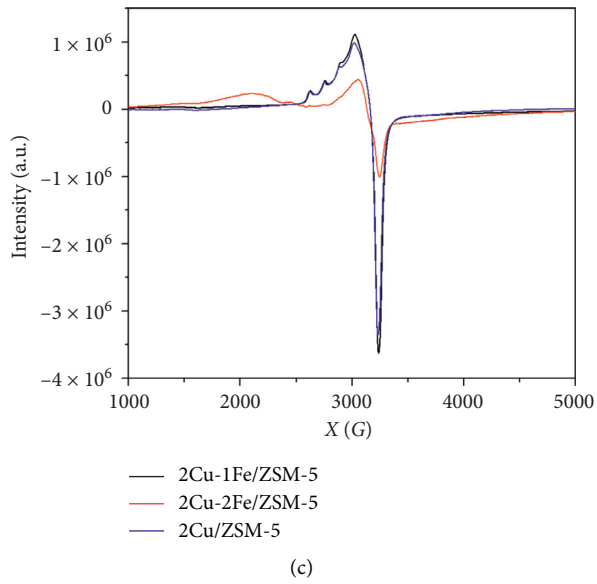

Figure 8: EPR spectra of series catalysts measured at -173°C of (a) Cu/ZSM-5, (b) Fe/ZSM-5, and (c) Cu-Fe/ZSM-5.

window of 450–550°C as seen in Figure 9(c) (defined as NO conversion more than 2Cu/ZSM-5 sample). Compared to both of these experiments, the findings in Figure 9(c) reveal that the 2Cu-1Fe/ZSM-5 sample shows the most potent catalyst. In specific, relative to 2Cu/ZSM-5, the conversion of NO_x over 2Cu-1Fe/ZSM-5 catalyst decreases marginally at low temperatures (below 250°C), accompanied by a rise in the range of 350–550°C. Notably, the NO_x removal yields still reached 75% at 550°C, suggesting that Cu-Fe/ZSM-5 catalysts have expanded the operating temperature window.

It is well known that NO_x conversion decrease with the reduction in N_2 selectivity at high temperatures is due to oxidation in NH_3 to unwanted N_2O formation. The NH_3 oxidation activity was also carried out for chosen catalysts. As seen in Figure 10, 2Cu/ZSM-5 and 2Cu-1Fe/ZSM-5 samples give the same curve shapes of NH_3 conversion. The reaction to ammonia oxidation begins at 225°C but happens at a low rate in the temperature range below 300°C. The NH_3 conversion is rising dramatically above this temperature. A singular copper catalyst shows the highest activity of NH_3 oxidation, while bimetal samples demonstrate the lower action. The Cu/ZSM-5 conversion was almost 100% at 550°C, while it was about 90% in the codoping Cu-Fe. Figure 9 also shows the catalytic behavior of Fe/ZSM-5 decomposing NH_3 catalysts that display an initial reaction temperature of 400°C and achieve just 35% with 550°C.

The reactions on the catalyst involve mainly the standard SCR and NH_3 oxidation reactions expressing

$$4NO + 4NH_3 + O_2 \longrightarrow 4N_2 + 6H_2O \quad (4)$$

$$4NH_3 + 3O_2 \longrightarrow 2N_2 + 6H_2O \quad (5)$$

As shown in Figures 9 and 10, the sample efficiency of the NH_3-SCR reaction has been slightly enhanced over the NH_3 oxidation reaction below 300°C, indicating a slight effect on catalytic activity in this temperature range due to the NH_3 oxidation reaction. A strong ammonia inhibition effect of iron heads to a limited NH_3-SCR performance below 350°C for the 2Cu-1Fe/ZSM-5 samples [13]. However, this catalyst's catalytic activity displayed an improvement in the range of 250–450°C, explained by the rise in the quantity of isolated Cu^{2+} ions identified as active sites for SCR reactions (Figures 7 and 8) [50]. Compared to Cu/ZSM-5, the 2Cu-1Fe/ZSM-5 sample could not increase its NH_3 oxidation activity. This may be explained by the decrease in the number of bulk CuO species that are expected to be extremely active for NH_3 oxidation in the bimetal study [55]. A reduction in the number of bulk CuO species on the surface with Fe and Cu prevents the NH_3 oxidation reaction. Consequently, the decrease in the NH_3 oxidation potential and increase in the sample catalytic activity of 2Cu-1Fe/ZSM-5 contributes by the small amount of oligomeric Fe_xO_y species and isolated Cu^{2+}.

In the 2Fe-2Cu/ZSM-5 sample, as discussed in EPR results, the oligomeric Fe^{3+} ions have replaced a small number of isolated Cu^{2+} ions, whereas Cu^{2+} isolated ions are readily combined with CuO_x species [6]. This means that the decrease in the isolated Cu^{2+} count (Figure 8(c)), surface area decreases, and ZSM5 pores volume (Table 2) by the aggregated Fe_2O_3 particles decreases 2Fe-2Cu/ZSM-5 sample SCR operation at lower and medium temperatures at below 400°C [56]. In the meantime, the increase in SCR performance above 400°C might affect an increased amount of oligomeric Fe_xO_y and Fe_2O_3 clusters in the sample.

The hydrothermal stability of catalysts is an essential problem for SCRs since the generation of heat during the process of regeneration of DPF must be dealt with [57]. To investigate this property, the 2Cu/ZSM-5 and 2Cu-1Fe/ZSM-5 catalysts were treated in 10% H_2O/air under a total flow rate of 1 L/min at 650°C and 750°C for 24 hours. Figure 11(a) depicts the SCR activity differences between

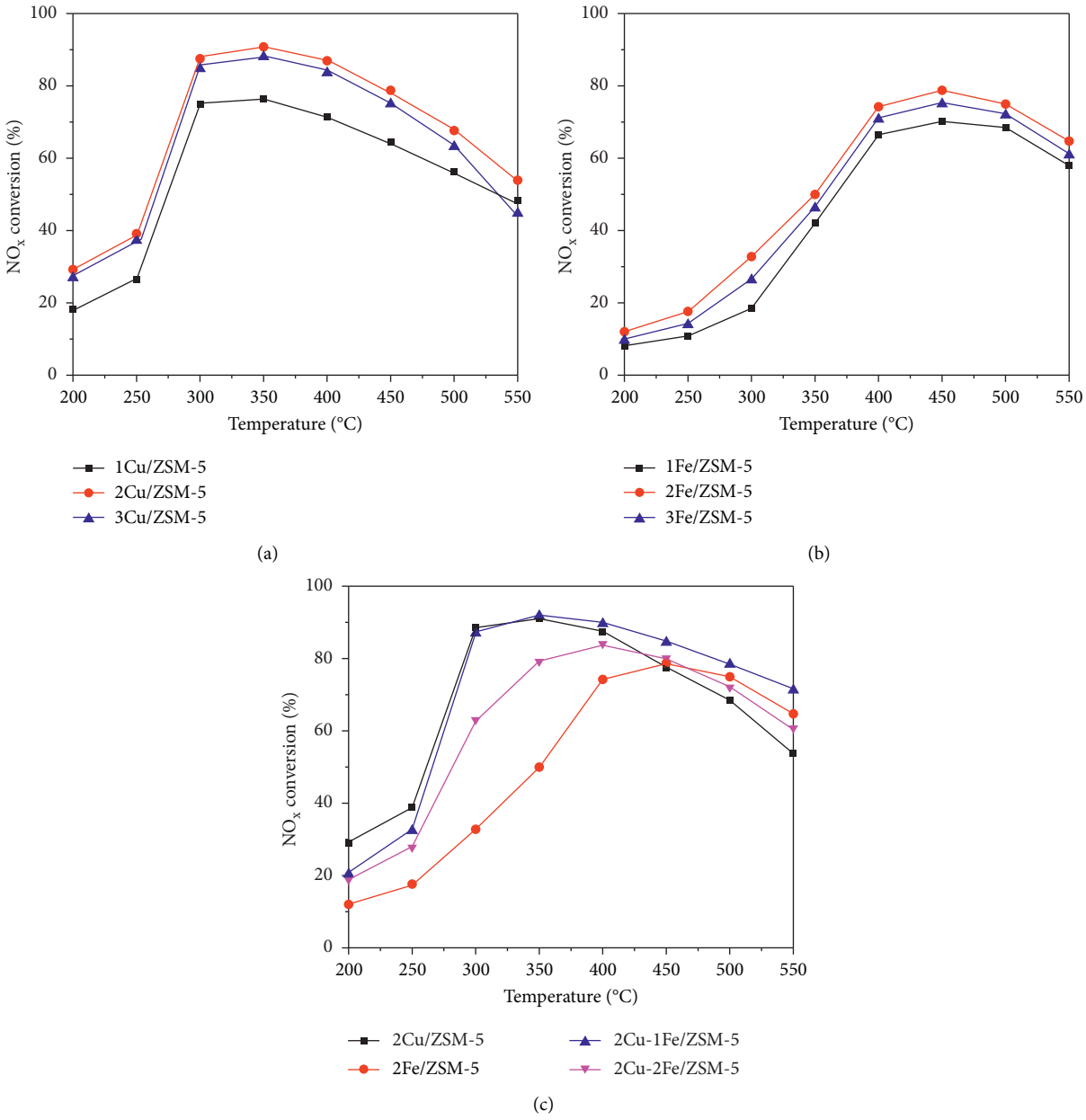

Figure 9: NO_x conversion during standard NH_3-SCR as a function temperature of (a) Cu/ZSM-5, (b) Fe/ZSM-5, and (c) Cu-Fe/ZSM-5.

fresh and hydrothermal aged samples, observing that the NO_x conversion of hydrothermally processed samples reduces the whole temperature range. In particular, both 2Cu-1Fe/ZSM-5_650°C and 2Cu-1Fe/ZSM-5_750°C achieved more than 60% NO_x conversion from 300 to 500°C. Both 2Cu-1Fe/ZSM-5 samples with two hydrothermal aging conditions have considerably higher NO_x conversion than 2Cu/ZSM-5_650°C, meaning that Cu-Fe/ZSM-5 is more stable and resistant to relatively harsh hydrothermal treatment than Cu/ZSM-5. To be more specific, XRD patterns of the fresh and hydrothermal aging catalysts are shown in Figure 11(b). The result deconvoluted that all the other catalysts have the MFI zeolite structure apart from the 2Cu/ZSM-5_750°C sample. This singular copper exchanged ZSM-5 catalyst appeared to be more sensitive to hydrothermal treatment since the collapse of the MFI structure occurred at 750°C. This framework damage could be probably due to the aggregation of copper species, which could affect negatively the stability of the structure and lead to the deterioration in catalytic activity on NH_3-SCR [18]. On the opposite, the hydrothermal treatment even at harsh conditions just had a negligible effect on the structure of 2Cu-1Fe/ZSM-5 samples. This insignificant effect on the bimetallic catalyst suggests that the addition of iron can help

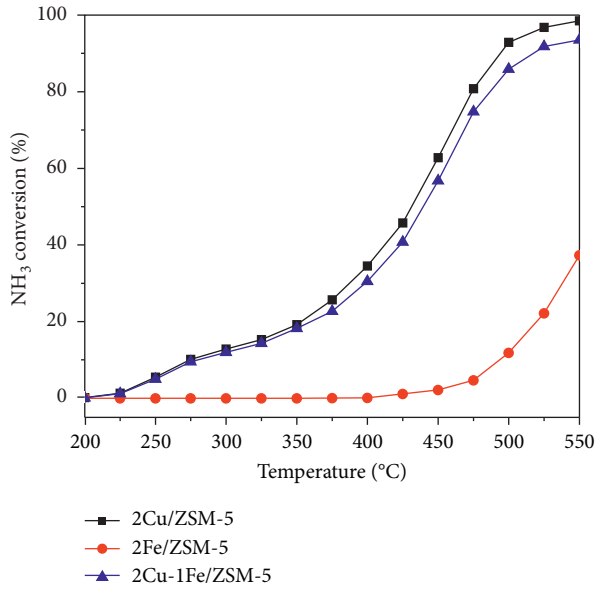

Figure 10: NH_3 conversion as a function of temperature during NH_3 oxidation experiment for the catalysts.

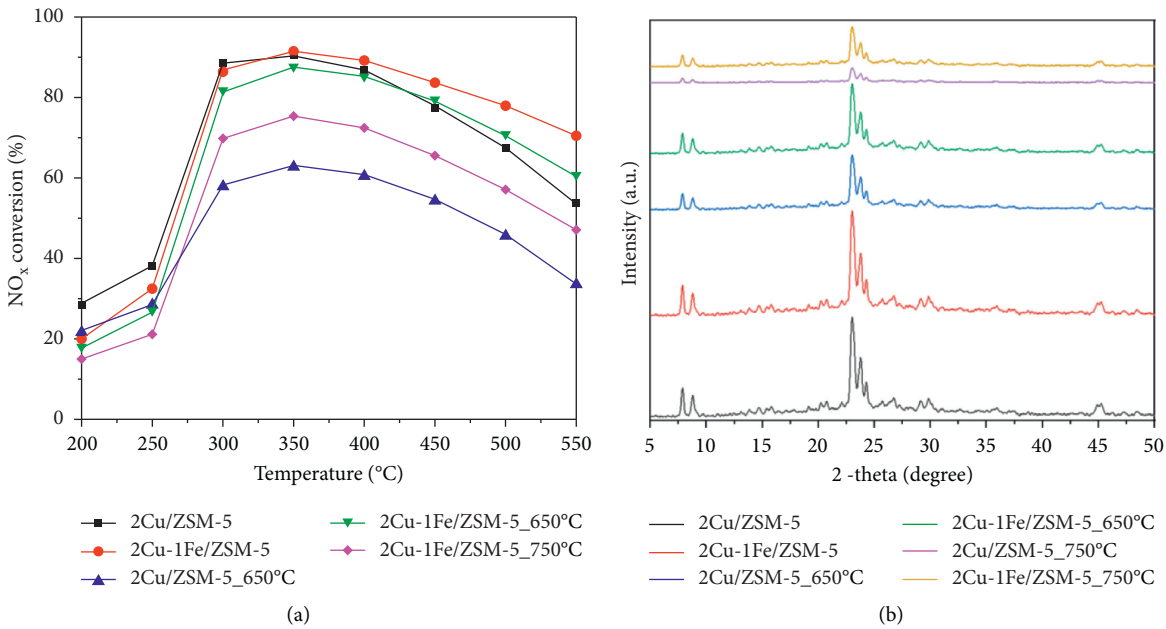

Figure 11: (a) NO_x conversion of Cu/ZSM-5 and Cu-Fe/ZSM-5 after hydrothermal aging and (b) XRD patterns of fresh and hydrothermal aging catalysts.

to stabilize the copper dispersion during aging; therefore, the increase in dispersing copper attends to be the primary explanation for the fact that the Cu-Fe/ZSM-5 catalysts improve hydrothermal stability.

4. Conclusion

In conclusion, hybrid Cu-Fe/ZSM-5 zeolites have been successfully synthesized using a liquid ion-exchange technique. Both catalysts systematically characterized the physicochemical properties by different techniques and were compared with mono Fe/ZSM-5, Cu/ZSM-5 zeolites developed using the same process. The XRD, FE-SEM, and N_2 adsorption-desorption also demonstrated that most of the physical structure and crystal of ZSM-5 remained while Cu and Fe are codoped. The H_2-TPR findings show that Cu-Fe/ZSM-5, owing to high-temperature redox capacities and abundance types of iron materials, has strong redox capability even over a broader temperature spectrum than Cu/ZSM-5. The UV-Vis DRS detected multiple active locations after Fe loading, namely, Fe^{3+} and Fe_xO_y, and a close relationship between Fe and Cu. The EPR results also confirm this. Compared to the Cu/ZSM-5 catalyst having the same amount of copper loading, the quantity of Cu^{2+} isolated was

increased when the required amount of Fe was included in the Cu-Fe/ZSM-5 catalyst. Besides, the increased number of Fe_xO_y oligomeric in this experiment profits from the NH_3-SCR reaction at high temperatures. Due to these characteristics, the Cu-Fe/ZSM-5 synthesized hybrid exhibits superior catalytic efficiency in the NH_3-SCR reaction., i.e., high NO conversion in a wide temperature window (350–550°C) and increase in N_2 selectivity. Our research offers an alternate NH_3-SCR catalyst for potential applications shortly.

Data Availability

X-ray diffraction, field emission scanning electron microscopy, energy-dispersive X-ray spectroscopy, nitrogen adsorption/desorption, UV-Vis diffuse reflectance spectroscopy, temperature-programmed desorption of ammonia, temperature-programmed reduction of hydrogen, and electron paramagnetic resonance methods used to support the findings of this study are included within the article.

Conflicts of Interest

The authors declare that they have no conflicts of interest.

Acknowledgments

This research was funded by the Vietnam National Foundation for Science and Technology Development (NAFOSTED) under grant no. 104.05–2018.306 and Vingroup Innovation Foundation (VINIF) under grant no. VINIF.2020.TS.124. This work has also been supported by the RoHan Project funded by the German Academic Exchange Service (DAAD, No. 57315854) and the Federal Ministry for Economic Cooperation and Development (BMZ) inside the framework "SDG Bilateral Graduate School Programme".

References

[1] J. Wang, H. Zhao, G. Haller, and Y. Li, "Recent advances in the selective catalytic reduction of NO_x with NH_3 on Cu-Chabazite catalysts," *Applied Catalysis B: Environmental*, vol. 202, pp. 346–354, 2017.

[2] M. Agote-Arán, I. Lezcano-González, A. G. Greenaway et al., "Operando XAFS studies reveals differences in the activity of Fe-species in MFI and CHA structures for the standard selective catalytic reduction of NO with NH_3," *Applied Catalysis A: General*, vol. 570, pp. 283–291, 2018.

[3] P. Granger and V. I. Parvulescu, "Catalytic NOxAbatement systems for mobile sources: from three-way to lean burn aftertreatment technologies," *Chemical Reviews*, vol. 111, no. 5, pp. 3155–3207, 2011.

[4] M. Zhu, J.-K. Lai, U. Tumuluri, M. E. Ford, Z. Wu, and I. E. Wachs, "Reaction pathways and kinetics for selective catalytic reduction (SCR) of acidic NOx emissions from power plants with NH3," *ACS Catalysis*, vol. 7, no. 12, pp. 8358–8361, 2017.

[5] U. Deka, I. Lezcano-Gonzalez, B. M. Weckhuysen, and A. M. Beale, "Local environment and nature of Cu active sites in zeolite-based catalysts for the selective catalytic reduction of NOx," *ACS Catalysis*, vol. 3, no. 3, pp. 413–427, 2013.

[6] T. Zhang, J. Li, J. Liu et al., "High activity and wide temperature window of Fe-Cu-SSZ-13 in the selective catalytic reduction of NO with ammonia," *AIChE Journal*, vol. 61, pp. 3825–3837, 2015.

[7] J. Liang, J. Tao, Y. Mi et al., "Unraveling the boosting low-temperature performance of ordered mesoporous Cu-SSZ-13 catalyst for NOx reduction," *Chemical Engineering & Technology*, vol. 409, Article ID 128238, 2021.

[8] A. Bellmann, H. Atia, U. Bentrup, and A. Brückner, "Mechanism of the selective reduction of NOx by methane over Co-ZSM-5," *Applied Catalysis B: Environmental*, vol. 230, pp. 184–193, 2018.

[9] Y. Xin, Q. Li, and Z. Zhang, "Zeolitic materials for DeNOx selective catalytic reduction," *ChemCatChem*, vol. 10, no. 1, pp. 29–41, 2017.

[10] C. Peng, R. Yan, H. Peng et al., "One-pot synthesis of layered mesoporous ZSM-5 plus Cu ion-exchange: enhanced NH3-SCR performance on Cu-ZSM-5 with hierarchical pore structures," *Journal of Hazardous Materials*, vol. 385, Article ID 121593, 2020.

[11] A. Grossale, I. Nova, and E. Tronconi, "Ammonia blocking of the "Fast SCR" reactivity over a commercial Fe-zeolite catalyst for Diesel exhaust aftertreatment," *Journal of Catalysis*, vol. 265, no. 2, pp. 141–147, 2009.

[12] M. Moreno-González, B. Hueso, M. Boronat, T. Blasco, and A. Corma, "Ammonia-containing species formed in Cu-chabazite as per in situ EPR, solid-state NMR, and DFT calculations," *The Journal of Physical Chemistry Letters*, vol. 6, no. 6, pp. 1011–1017, 2015.

[13] M. Schwidder, M. Kumar, K. Klementiev, M. Pohl, A. Bruckner, and W. Grunert, "Selective reduction of NO with Fe-ZSM-5 catalysts of low Fe contentI. Relations between active site structure and catalytic performance," *Journal of Catalysis*, vol. 231, no. 2, pp. 314–330, 2005.

[14] M. S. Kumar, M. Schwidder, W. Grünert, and A. Brückner, "On the nature of different iron sites and their catalytic role in Fe-ZSM-5 DeNOx catalysts: new insights by a combined EPR and UV/VIS spectroscopic approach," *Journal of Catalysis*, vol. 227, no. 2, pp. 384–397, 2004.

[15] E. J. M. Hensen, Q. Zhu, M. M. R. M. Hendrix et al., "Effect of high-temperature treatment on Fe/ZSM-5 prepared by chemical vapor deposition of FeCl3I. Physicochemical characterization," *Journal of Catalysis*, vol. 221, no. 2, pp. 560–574, 2004.

[16] T. Zhang, J. Liu, D. Wang et al., "Selective catalytic reduction of NO with NH3 over HZSM-5-supported Fe-Cu nanocomposite catalysts: the Fe-Cu bimetallic effect," *Applied Catalysis B: Environmental*, vol. 148-149, pp. 520–531, 2014a.

[17] R. Zhang, Y. Li, and T. Zhen, "Ammonia selective catalytic reduction of NO over Fe/Cu-SSZ-13," *RSC Advances*, vol. 4, no. 94, pp. 52130–52139, 2014b.

[18] T. Doan, P. Dam, K. Nguyen, TH. Vuong, M. T. Le, and T. H. Pham, "Copper-iron bimetal ion-exchanged SAPO-34 for NH3-SCR of NOx," *Catalysts*, vol. 10, no. 3, p. 321, 2020.

[19] A. R. Fahami, T. Günter, D. E. Doronkin et al., "The dynamic nature of Cu sites in Cu-SSZ-13 and the origin of the seagull NOx conversion profile during NH3-SCR," *Reaction Chemistry & Engineering*, vol. 4, pp. 1000–1018, 2019.

[20] P. Nakhostin Panahi, D. Salari, A. Niaei, and S. M. Mousavi, "Study of M-ZSM-5 nanocatalysts (M: Cu, Mn, Fe, Co . . .) for selective catalytic reduction of NO with NH3: process optimization by Taguchi method) for selective catalytic reduction

of NO with NH3: process optimization by Taguchi method," *Chinese Journal of Chemical Engineering*, vol. 23, no. 10, pp. 1647–1654, 2015.

[21] T. Doan, A. Dang, D. Nguyen et al., "Influence of aluminum sources on synthesis of SAPO-34 and NH3-SCR of NOx by as-prepared Cu/SAPO-34 catalysts," *Catalysis in Industry*, vol. 20, no. 5, p. 373, 2020.

[22] Y. Yue, B. Liu, N. Lv et al., "Direct synthesis of hierarchical FeCu-ZSM-5 zeolite with wide temperature window in selective catalytic reduction of NO by NH3," *ChemCatChem*, vol. 11, pp. 4744–4754, 2019.

[23] S. Prodinger, M. A. Derewinski, Y. Wang et al., "Sub-micron Cu/SSZ-13: synthesis and application as selective catalytic reduction (SCR) catalysts," *Applied Catalysis B: Environmental*, vol. 201, pp. 461–469, 2017.

[24] P. N. Panahi, D. Salari, A. Niaei, and S. M. Mousavi, "NO reduction over nanostructure M-Cu/ZSM-5 (M: Cr, Mn, Co and Fe) bimetallic catalysts and optimization of catalyst preparation by RSM," *Journal of Industrial and Engineering Chemistry*, vol. 19, no. 6, pp. 1793–1799, 2013.

[25] P. Nakhostin Panahi, "Comparative study of ZSM-5 supported transition metal (Cu, Mn, Co, and Fe) nanocatalysts in the selective catalytic reduction of NO with NH3," *Environmental Progress & Sustainable Energy*, vol. 36, no. 4, pp. 1049–1055, 2017.

[26] Z. Wu, B. Jiang, and Y. Liu, "Effect of transition metals addition on the catalyst of manganese/titania for low-temperature selective catalytic reduction of nitric oxide with ammonia," *Applied Catalysis B: Environmental*, vol. 79, no. 4, pp. 347–355, 2008.

[27] R. Long and R. Yang, "Temperature-programmed desorption/surface reaction (TPD/TPSR) study of Fe-exchanged ZSM-5 for selective catalytic reduction of nitric oxide by ammonia," *Journal of Catalysis*, vol. 198, no. 1, pp. 20–28, 2001.

[28] L. J. Lobree, I.-C. Hwang, J. A. Reimer, and A. T. Bell, "Investigations of the state of Fe in H–ZSM-5," *Journal of Catalysis*, vol. 186, no. 2, pp. 242–253, 1999.

[29] H. Karge, G. Ohlmann, H. Pfeifer, and R. Fricke, *Catalysis and Adsorption by Zeolites*, Elsevie, Amsterdam, Netherlands, 1991.

[30] P. Boroń, L. Chmielarz, J. Gurgul et al., "Influence of iron state and acidity of zeolites on the catalytic activity of FeHBEA, FeHZSM-5 and FeHMOR in SCR of NO with NH3 and N2O decomposition," *Microporous and Mesoporous Materials*, vol. 203, pp. 73–85, 2015.

[31] M. Rostamizadeh and F. Yaripour, "Bifunctional and bimetallic Fe/ZSM-5 nanocatalysts for methanol to olefin reaction," *Fuel*, vol. 181, pp. 537–546, 2016.

[32] S. Deng, K. Zhuang, B. Xu, Y. Ding, L. Yu, and Y. Fan, "Promotional effect of iron oxide on the catalytic properties of Fe-MnOx/TiO2 (anatase) catalysts for the SCR reaction at low temperatures," *Catalysis Science & Technology*, vol. 6, no. 6, pp. 1772–1778, 2016.

[33] H. Xiaosheng, Z. Guodong, D. Fang, and T. Zhicheng, "An environmentally friendly wide temperature CeWTiOx catalyst with superior performance for the selective catalytic reduction NOx with NH3," *Journal of Industrial and Engineering Chemistry*, vol. 69, pp. 66–76, 2018.

[34] W. Gruenert, N. W. Hayes, R. W. Joyner, E. S. Shpiro, M. R. H. Siddiqui, and G. N. Baeva, "Structure, chemistry, and activity of Cu-ZSM-5 catalysts for the selective reduction of NOx in the presence of oxygen," *The Journal of Physical Chemistry*, vol. 98, no. 42, 1994.

[35] H. Wang, J. Jia, S. Liu et al., "Highly efficient NO abatement over Cu-ZSM-5 with special nanosheet features," *Environmental Science & Technology*, vol. 55, no. 8, pp. 5422–5434, 2021.

[36] G. Qi and R. T. Yang, "Ultra-active Fe/ZSM-5 catalyst for selective catalytic reduction of nitric oxide with ammonia," *Applied Catalysis B: Environmental*, vol. 60, no. 1-2, pp. 13–22, 2005.

[37] R. Q. Long and R. T. Yang, "Characterization of Fe-ZSM-5 catalyst for selective catalytic reduction of nitric oxide by ammonia," *Journal of Catalysis*, vol. 194, no. 1, pp. 80–90, 2000.

[38] S. S. R. Putluru, L. Schill, A. D. Jensen, and R. S. N. Fehrmann, "Selective catalytic reduction of NOx with NH3 on Cu-, Fe-, and Mn-zeolites prepared by impregnation: comparison of activity and hydrothermal stability," *Journal of Chemistry*, vol. 2018, Article ID 8614747, 11 pages, 2018.

[39] A. Guzmán-Vargas, G. Delahay, B. Coq, E. Lima, P. Bosch, and J.-C. Jumas, "Influence of the preparation method on the properties of Fe-ZSM-5 for the selective catalytic reduction of NO by n-decane," *Catalysis Today*, vol. 107, pp. 94–99, 2005.

[40] J. Pérez-Ramírez, G. Mul, F. Kapteijn et al., "Physicochemical characterization of isomorphously substituted FeZSM-5 during activation," *Journal of Catalysis*, vol. 207, no. 1, pp. 113–126, 2002.

[41] K. Krishna and M. Makkee, "Preparation of Fe-ZSM-5 with enhanced activity and stability for SCR of NOx," *Catalysis Today*, vol. 114, no. 1, pp. 23–30, 2006.

[42] J. Teržan, P. Djinović, J. Zavašnik et al., "Alkali and earth alkali modified CuOx/SiO2 catalysts for propylene partial oxidation: what determines the selectivity?" *Applied Catalysis B: Environmental*, vol. 237, pp. 214–227, 2018.

[43] I. Ellmers, R. Pérez Vélez, U. Bentrup, W. Schwieger, A. Brückner, and W. Grünert, "SCR and NO oxidation over Fe-ZSM-5 – the influence of the Fe content," *Catalysis Today*, vol. 258, pp. 337–346, 2015.

[44] S. Bordiga, R. Buzzoni, F. Geobaldo et al., "Structure and reactivity of framework and extraframework iron in Fe-silicalite as investigated by spectroscopic and physicochemical methods," *Journal of Catalysis*, vol. 158, no. 2, pp. 486–501, 1996.

[45] K. Sun, H. Xia, Z. Feng, R. Vansanten, E. Hensen, and C. Li, "Active sites in Fe/ZSM-5 for nitrous oxide decomposition and benzene hydroxylation with nitrous oxide," *Journal of Catalysis*, vol. 254, no. 2, pp. 383–396, 2008.

[46] H. Jouini, I. Mejri, C. Petitto et al., "Characterization and NH3-SCR reactivity of Cu-Fe-ZSM-5 catalysts prepared by solid state ion exchange: the metal exchange order effect," *Microporous and Mesoporous Materials*, vol. 260, pp. 217–226, 2018.

[47] X. Liao, Z. Hu, L. Ma, Q. Hao, and S. Lu, "Cu location onto spherical SiO2@Mn make a profound difference for catalytic oxidative removal Na2S in waste water with air as an oxidant at ambient conditions," *Chemical Engineering Journal*, vol. 351, pp. 280–294, 2018.

[48] F. Heinrich, C. Schmidt, E. Löffler, M. Menzel, and W. Grünert, "Fe–ZSM-5 catalysts for the selective reduction of NO by isobutane - the problem of the active sites," *Journal of Catalysis*, vol. 212, no. 2, pp. 157–172, 2002.

[49] C. Lamberti, S. Bordiga, M. Salvalaggio et al., "XAFS, IR, and UV–Vis study of the CuI environment in CuI-ZSM-5," *The Journal of Physical Chemistry B*, vol. 101, no. 3, pp. 344–360, 1997.

[50] A. M. Beale, F. Gao, I. Lezcano-Gonzalez, C. H. F. Peden, and J. Szanyi, "Recent advances in automotive catalysis for NOx emission control by small-pore microporous materials," *Chemical Society Reviews*, vol. 44, no. 20, pp. 7371–7405, 2015.

[51] X. Dong, J. Wang, H. Zhao, and Y. Li, "The promotion effect of CeOx on Cu-SAPO-34 catalyst for selective catalytic reduction of NOx with ammonia," *Catalysis Today*, vol. 258, pp. 28–34, 2015.

[52] S. Stoll and A. Schweiger, "EasySpin, a comprehensive software package for spectral simulation and analysis in EPR," *Journal of Magnetic Resonance*, vol. 178, no. 1, pp. 42–55, 2006.

[53] A. Godiksen, P. N. R. Vennestrøm, S. B. Rasmussen, and S. Mossin, "Identification and quantification of copper sites in zeolites by electron paramagnetic resonance spectroscopy," *Topics in Catalysis*, vol. 60, no. 1-2, pp. 13–29, 2016.

[54] M. Høj, M. J. Beier, J.-D. Grunwaldt, and S. Dahl, "The role of monomeric iron during the selective catalytic reduction of NOx by NH3 over Fe-BEA zeolite catalysts," *Applied Catalysis B: Environmental*, vol. 93, no. 1-2, pp. 166–176, 2009.

[55] T. Yu, J. Wang, Y. Huang, M. Shen, W. Li, and J. Wang, "NH3 oxidation mechanism over Cu/SAPO-34 catalysts prepared by different methods," *ChemCatChem*, vol. 6, no. 7, pp. 2074–2083, 2014.

[56] F. Gao, E. D. Walter, E. M. Karp et al., "Structure–activity relationships in NH3-SCR over Cu-SSZ-13 as probed by reaction kinetics and EPR studies," *Journal of Catalysis*, vol. 300, pp. 20–29, 2013.

[57] J. H. Park, H. J. Park, J. H. Baik et al., "Hydrothermal stability of CuZSM5 catalyst in reducing NO by NH3 for the urea selective catalytic reduction process," *Journal of Catalysis*, vol. 240, pp. 47–57, 2006.